Lineshape Models in Inner-shell Photoelectron Spectra of Free Molecules and Clusters

Mahmoud Abu-samha

Department of Chemistry
University of Bergen

· 2006 ·

Abstract

Investigating the nature of molecules and clusters is of paramount importance for our understanding of the composition and the properties of matter. X-ray photoelectron spectroscopy is one of the most powerful techniques for obtaining information at the fundamental level about molecules and clusters. Our interest in this particular kind of spectroscopy derives from its ability to probe individual atoms in a molecule and their chemical surrounding. Experimental core-level photoelectron spectra show great complexity, even for simple molecules. Hence, developing theoretical lineshapes to model and interpret experimental spectra is necessary. This thesis is devoted to the development of novel theoretical methods for modeling x-ray photoelectron spectra of molecules and clusters. It also demonstrates how these models can be used as means of extracting chemical information from experimental spectra.

In this thesis, the carbon 1s photoelectron spectrum of gas-phase ethanol has been investigated by calculations, and found to be significantly influenced by the presence of a conformational equilibrium. Furthermore, theoretical models have been used to analyze inner-shell photoelectron spectra of clusters made up of either argon, methane, or methanol molecules. With the help of these models we have been able to interpret the experimental spectra in terms of chemical shifts, vibrations, and the chemical surrounding of atoms (molecules) in the cluster. The results are very interesting and will, hopefully, contribute to the development of the current understanding of the structures and properties of clusters.

Acknowledgments

I wish to express my sincere gratitude to all the people who have contributed to this thesis in one way or another.

First of all, I would like to thank my supervisor, Prof. Knut J. Børve, for all his guidance, encouragement and enthusiasm, and for being a source of inspiration and friendship. I must say that without his help this thesis would never have been completed.

I would like to thank as well my second supervisor, Prof. Leif. J. Sæthre, for his never-failing support and assistance.

I would like to take the opportunity to thank my colleagues and friends in the electron spectroscopy group at the University of Bergen, in particular Alf Holme, Jarle Harnes, Maria Gundersen, and Velaug Myrseth Oltedal, for helpful discussions and supportive environment.

I want to thank my colleagues in the electron spectroscopy group in Uppsala University, Henrik Bergersen, Gunnar Öhrwall, Torbjörn Rander, Andreas Lindblad, Ricardo Marinho, Denis Céolin, Prof. Olle Björneholm, and Prof. Svante Svensson, for a very fruitful and stimulating cooperation.

I wish to thank Prof. T. Darrah Thomas for his cooperation, and for being nice to me during my research stay in Corvallis.

I thank the staff members at MaxLab, most notably Maxim Tchaplyguine, for their assistance during our stay at Maxlab.

I thank my family and friends for being supportive.

Finally, a lot of thanks to The Norwegian State Educational Loan Fund for the financial support, and to The Norwegian Metacenter For Computational Science (NOTUR) for computational facilities.

Bergen August 30, 2006
M. Abu-samha

Contents

List of Papers

This thesis is based on the following scientific papers.

I Conformational Effects in Inner-Shell Photoelectron Spectroscopy of Ethanol.
M. Abu-samha, K. J. Børve, L. J. Sæthre, and T. D. Thomas.
Physical Review Letters **95**, 103002 (2005).

II The C1s photoelectron spectrum of ethanol: Franck-Condon transitions in a system with large-amplitude anharmonic vibrations coupled to a harmonic-oscillator bath.
M. Abu-samha and K. J. Børve.
Manuscript.

III Size of neutral argon clusters from core-level photoelectron spectroscopy.
H. Bergersen, M. Abu-samha, J. Harnes, O. Björneholm, S. Svensson, L. J. Sæthre and K. J. Børve.
Physical Chemistry Chemical Physics **8** 1891 (2006).

IV First observation of vibrations in core-level photoelectron spectra of free neutral molecular clusters.
H. Bergersen, M. Abu-samha, A. Lindblad, R. T. T. Marinho, D. Céolin, G. Öhrwall, L. J. Sæthre, M. Tchaplyguine, K. J. Børve, S. Svensson, and O. Björneholm.
Chemical Physics Letters, submitted.

V Lineshapes in carbon 1s photoelectron spectra of methanol clusters.
M. Abu-samha, K. J. Børve, L. J. Sæthre, G. Öhrwall, H. Bergersen, T. Rander, O. Björneholm, and M. Tchaplyguine.
Physical Chemistry Chemical Physics **8** 2473 (2006).

Chapter 1

Introduction

Atoms and molecules are the building units of everything. It is therefore obvious that the investigations of atoms and molecules have the potential to help us to understand and to design materials of all kind. Still, the properties of atoms and molecules are different from the properties of matter we confront in daily life, that is, the properties of the condensed phases surpass and are different from the building units of which they consist. Hence, it is rather interesting to investigate how the chemical and physical properties of condensed materials relate to those of the building units.

The evolution of physical and chemical properties from the building units to condensed matter can be mapped semi-continuously by studying clusters. Clusters are finite aggregates of atoms or molecules, that range in size from the dimer up to several tens of thousands of units. In this sense they constitute intermediates between free atoms and molecules, with clearly defined energy states, and condensed matter where these states form continua or bands.

Investigations of electronic and geometric structures of atoms, molecules, and clusters are thus fundamental to understand the composition and the properties of matter. The electronic structure is of particular interest because it helps determining most physical and chemical properties. Our current understanding of the electronic structure of matter is largely based on the study of electronic spectra. The electronic spectra of atoms for instance provide evidence of the quantum nature of matter at the atomic level. In the same way, the electronic spectra of molecules give information about their electronic structures, the strengths of their bonds, and other information that is needed to account for chemical reactions. However, the electronic spectra rarely give direct information about molecular structures. This is simply because the electronic spectra are very complex, consisting in most cases of broad bands.

Core-level spectroscopy is an established tool for obtaining information about the electronic and geometric structures of isolated atoms, molecules, surfaces and solids. The techniques include x-ray photoelectron spectroscopy (XPS), x-ray absorption spectroscopy (XAS), Auger electron spectroscopy (AES), and x-ray emission spectroscopy (XES). Due to the atomic character of the core orbitals, core-level energies are specific to each element. In x-ray photoelectron spectroscopy, a photoelectron is removed from the sample by a photon. The kinetic energy of the photoelectron is analyzed by means of

an electron spectrometer. At low-to-medium kinetic energies, the mean free path of the photoelectron is very limited, so the measurements are intrinsically surface sensitive. X-ray photoelectron spectroscopy is very sensitive to the local surroundings of the core hole site, thus it allows for chemical-state specific investigations when exploiting the so-called chemical shift in core ionizations.

In our group we use synchrotron-based x-ray photoelectron spectroscopy. Synchrotron radiation is about five orders of magnitude brighter than any conventional x-ray tubes. With the high brightness x-ray beams produced by the third generation synchrotrons and the better resolution due to the development of electron spectrometers, one can determine the ionization energies of core electrons to within a few meV. At this level of precision, one observes fine structure in x-ray photoelectron spectra at the sub 100 meV scale (Svensson 2005, Hergenhahn 2004). Quantum mechanics is necessary for the interpretation of fine structure in high-resolution spectra. Thus, theory together with experimental spectra form a basic tool for our understanding of physical mechanisms that determine the property of matter.

The high photon flux has made it possible to study samples with very low densities, such as clusters where the sample densities are 5-7 orders of magnitude smaller than for stable molecules. By exploiting the core-level photoelectron spectra of clusters of different sizes, it may be possible to gain knowledge at the fundamental level concerning the size-dependent evolution of physical and chemical properties. However, the spectra are in many cases difficult to interpret. Hence, it is rather necessary to compare the experimental spectra to theoretical models that represent well-defined bonding regimes in clusters.

The aim of this thesis is to develop novel computational models for analyzing x-ray photoelectron spectra of free molecules and clusters, and to use these models to examine selected representative systems. In particular, we see the development of these theoretical tools for spectral analysis as a way of promoting and advancing x-ray photoelectron spectroscopy as a technique for exploring clusters and obtaining information about their geometries and intermolecular bonding mechanisms.

The development and applications of theoretical tools for analyzing inner-shell photoelectron spectra of free molecules led to an important discovery, in that for the first time one has found evidence for a conformational equilibrium in such spectra. The theory development that led to this result is presented in papers I and II.

The major part of this thesis focuses on the development of a new toolkit for analyzing inner-shell photoelectron spectra of rare-gas and molecular clusters. Our work in this field is presented in papers III to V. In these papers, we address a multitude of issues regarding geometric structures and chemical shifts in core ionization. Moreover, we try to resolve other issues such estimating cluster sizes and size-distribution functions. First, we study argon clusters. These are systems of limited chemical interest, yet

interesting in their own right. Next, we consider methane clusters whose intermolecular bonding pattern is similar to that of argon. Then we go on to study methanol clusters, where the intermolecular bonding mechanism is rather complicated. In these studies, the theoretical models vary from being very simple to very complex depending on the spectra in question and the level of information required.

The experimental measurements have been performed at beamline I411 at MAX-II synchrotron facility in Lund, Sweden. The experimental results presented in this thesis are a product of collaboration between our group and the surface physics group in Uppsala University, Sweden.

The thesis is organised in the following way: Chapter 2 gives a brief introduction to the technique of x-ray photoelectron spectroscopy. In chapter 3 we discuss the aspects of lineshape modeling. Chapter 4 provides the reader with the theoretical and computational models employed in this thesis. The main results are given in chapters 5 and 6. The conclusions are given in chapter 7.

Chapter 2

X-ray Photoelectron Spectroscopy

The photoelectric effect is the emission of electrons from matter upon the absorption of electromagnetic radiation. This phenomenon was detected by Hertz in 1887. In the following years, Einstein was able to interpret the phenomenon by invoking the quantum nature of light. The basic equation governing the interaction of electromagnetic radiation with the matter is

$$h\nu = IE + KE \tag{2.1}$$

Here, h is Planck's constant, ν is the frequency of the electromagnetic radiation, KE is the kinetic energy of the emitted electrons, and IE is the energy needed to get the electrons out of the matter. Equation 2.1 was the starting point when Siegbahn and his research group developed modern x-ray photoelectron spectroscopy (XPS) in the 1950's.

In XPS, the sample is irradiated by x-ray photons, and core electrons are ejected. The departing electrons are analyzed with respect to their kinetic energy by an electrostatic analyzer. When an XPS experiment is performed on gas-phase samples, the ejected electrons escape freely into the vacuum. On the contrary, electrons ejected from condensed materials are likely to be captured by the surrounding matter, unless the probed atom is near the surface. How near depends on the kinetic energy of electrons. In the kinetic energy range of 10-2000 eV, the escape depth of the electrons is below 100 Å (Hüfner 1996). This technique is therefore suited to probe the surface region of condensed materials.

If one knows the energy of the incident photons and measures the kinetic energy of the ejected electrons, one will obtain the ionization energy by means of Eq. 2.1. Thus XPS measures the energy difference between the total energies of a state with N electrons E_i^N and one with N-1 electrons E_f^{N-1}. In mathematical formulation,

$$IE = E_f^{N-1} - E_i^N. \tag{2.2}$$

The ionization energy can be computed by theoretical means. A common approach in calculations of ionization energies is Koopmans' approximation, which states that the ionization energy equals the negative energy of the orbital from which the electron is ionized. In general, Koopmans' ionization energies are reasonable first approximations to experimental values. A more adequate approach is to calculate the difference in total energies between the neutral and the ionized species. However, the description of a

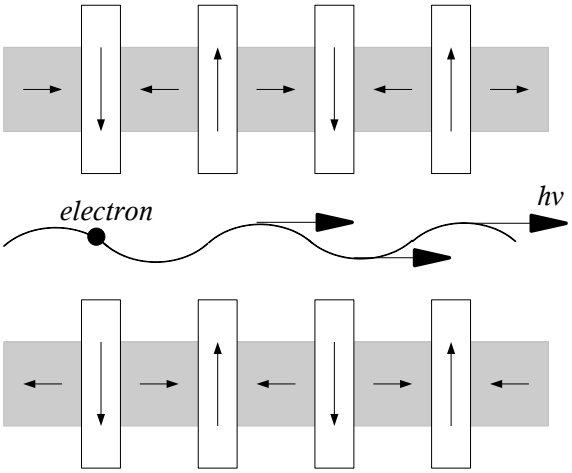

Figure 2.1: *Illustration of undulator radiation that is generated by electrons traversing a periodic magnetic structure.*

core-hole state is by no means trivial. In chapter 4 we present some of the approximations that one can employ in these calculations.

2.1 Experimental Aspect

The experimental data presented in this thesis were obtained at beamline I411, Maxlab third-generation synchrotron facility, Lund, Sweden.

Synchrotrons are huge machines used to accelerate sub-atomic particles to speeds near the speed of light (Attwood 2000). When the relativistic particles change their direction, by means of a magnetic field, they emit electromagnetic radiation. The first-generation synchrotrons were not built for this purpose, but for nuclear experiment, and the produced radiation was considered as a by-product. However, with the rapid expansion of the field, storage rings are now dedicated for the production of synchrotron radiation. Furthermore, novel radiation sources such as undulators and wigglers have been developed.

Synchrotron radiation is utilized by means of a beamline. The main components of a beamline are an undulator, a monochromator, and the end station (Jurvansuu 2000). Undulators are periodic magnetic structures with relatively weak magnetic fields. Schematic diagram of an undulator is shown in Figure 2.1. Relativistic electrons traversing the periodic magnet structure are forced to undergo oscillations and radiate photons in a narrow cone tangent to their path. The generated radiation is peaked in the soft x-

ray region. The undulator radiation can be extremely bright and partially coherent.

The undulator is followed by a monochromator that filter the radiation and select a spectral width. The monochromator installed at I411 is a modified version of the SX 700 plane grating monochromator (Petersen and Baumgärtel 1980, Nyholm et al. 1986). This monochromator type incorporates only three optical elements; a large plane mirror, a plane diffraction grating and a focusing mirror. The monochromator resolution is represented by a Gaussian distribution with a width determined by the monochromator exit slit.

The monochromated radiation is directed to the sample compartment at the end station. The end station is very versatile as it is adapted to handle gas phase, liquid phase and solid phase samples. It is equipped with a Scienta SES 200 electron spectrometer, which consists mainly of: an electron lens, a hemispherical electron energy analyzer, and a detector (Mårtensson et al. 1994). The spectrometer is rotable around the photon beam, thus making angle-resolved high resolution electron spectroscopy possible for various kinds of samples. The spectrometer resolution can be described by a Gaussian with a fwhm proportional to the width of the analyzer's entrance slit and its radius.

Chapter 3

Aspects of Lineshape Modeling

The high resolution power made possible at dedicated third-generation synchrotron facilities has revealed a new layer of information in core-level photoelectron spectra. In parallel with the experimental progress, theoretical tools have been developed for modeling and analyzing experimental inner-shell photoelectron spectra of atoms, molecules, and clusters. In this chapter, we discuss various mechanisms of fine structure and line broadening in core-level photoelectron spectroscopy, and present theoretical models that describe inner-shell photoelectron spectra of atoms, molecules, and clusters.

3.1 Fine structure in XPS

3.1.1 Chemical shift

In the investigation of molecules and clusters, we are interested in the change in ionization energy of a particular atom caused by the chemical surrounding. This energy difference is called the chemical shift. Chemical shifts have been observed in x-ray photoelectron spectroscopy as either a peak splitting or an extra line broadening, depending on a number of factors. These include the width of the peaks in question, the chemical surrounding of the probed atom, and the instrumental resolution.

Chemical shifts in core-level ionization energies provide us with information about the chemistry of molecules. In our group we have a long standing experience in the use of chemical shifts in carbon 1s ionization energy in the analysis of chemical reactivity of organic molecules (Sæthre et al. 1989, Carroll et al. 2006).

3.1.2 Vibrational structure

Core ionization of a polyatomic molecule causes the nuclei to break into vibration. The first observation of nuclear vibrations was in the carbon 1s photoelectron spectrum of methane, more than three decades ago (Gelius et al. 1974). The experiment was performed using monochromated AlKα radiation as a light source, and the instrumental resolution was limited to 400 meV. So the vibrational structure was not fully resolved.

In the following years, the carbon 1s ionization energy and the vibrational splittings in methane spectra have been accurately determined (Asplund et al. 1985).

Nowadays, x-ray photoelectron spectroscopy have reached a state where the vibrational fine-structure can be used to explore the nuclear dynamics following ionization, which is a rich source of information about the initial and final electronic states involved in the process. The theoretical analysis of the vibrational structure is based on the Franck-Condon principle.

Franck-Condon principle

The rate of photon absorption between initial state $|i\rangle$ and final state $|f\rangle$ is

$$W = \frac{2\pi}{\hbar^2} g(w_{fi}) \mid \mathbf{E_0} \cdot \langle f \mid \vec{\mu} \mid i \rangle \mid^2 \tag{3.1}$$

where $g(w_{fi})$ is the intensity of the photon source at the frequency of the transition under study, $\mathbf{E_0}$ is the electric field vector, and $\vec{\mu}$ is the electric dipole moment. The explicit form of the transition dipole moment is

$$\begin{aligned} \langle f \mid \vec{\mu} \mid i \rangle = & \int \psi_f^* (\mathbf{R}) \left[\int \phi_f^* (\mathbf{r}; \mathbf{R}) \, \vec{\mu}_e \phi_i (\mathbf{r}; \mathbf{R}) \, d\tau_e \right] \psi_i (\mathbf{R}) \, d\tau_n \\ & + \int \phi_f^* (\mathbf{r}; \mathbf{R}) \left[\int \psi_f^* (\mathbf{R}) \, \vec{\mu}_n \psi_i (\mathbf{R}) \, d\tau_n \right] \phi_i (\mathbf{r}; \mathbf{R}) \, d\tau_e \end{aligned} \tag{3.2}$$

where $\phi(\mathbf{r}; \mathbf{R})$ is the electronic- and $\psi(\mathbf{R})$ is the nuclear wavefunction, and $\vec{\mu}_e$ and $\vec{\mu}_n$ are the electronic- and the nuclear components of the transition dipole vector, respectively. Since the electronic states are orthogonal to one another for each selected value of $\mathbf{R}$, the second integral in Eq. 3.2 is zero. Therefore, equation 3.2 becomes

$$\langle f \mid \vec{\mu} \mid i \rangle = \int \phi_f^* (\mathbf{r}; \mathbf{R}) \, \vec{\mu}_e \phi_i (\mathbf{r}; \mathbf{R}) \, d\tau_e \int \psi_f^* (\mathbf{R}) \, \psi_i (\mathbf{R}) \, d\tau_n \tag{3.3}$$

where $\int \psi_f^* (\mathbf{R}) \, \psi_i (\mathbf{R}) \, d\tau_n$ is the overlap integral between the two nuclear wavefunctions (vibrational states), in their respective electronic states. The squares of these integrals are called Franck-Condon factors. These factors play important role in determining the relative intensities of various vibrational progressions observed in experimental spectra.

The Franck-Condon factors are very sensitive to the geometrical relaxation following electronic excitation/ionization. For instance, the larger the differences between the initial- and final-state potentials the broader will be the Franck-Condon profile.

Vibrational structure in XPS of molecules

The vibrational Schrödinger equation for a nonlinear N-atomic molecule may be written in atomic units as

$$\left[-\frac{1}{2}\sum_{j=1}^{3N-6}\frac{\partial^2}{\partial Q_j^2}+U(Q_1,Q_2,\ldots,Q_N)\right]\psi_n(Q_1,Q_2,\ldots,Q_N) \tag{3.4}$$

where Q_j is the jth mass-weighted normal coordinate, described by (Wilson et al. 1980)

$$Q_j=\sum_{r}^{3N} L_{rj}M_r^{\frac{1}{2}}\Delta x_r \tag{3.5}$$

where $\mathbf{L}$ is a unitary matrix, Δx_r is the cartesian displacement of the rth atom from equilibrium position, and M_r is its mass.

In the harmonic approximation, the vibrational wavefunction is written as:

$$\psi_n(\mathbf{Q})=\exp\left(-\frac{1}{2}\mathbf{Q}^{\dagger}\mathbf{\Gamma}\mathbf{Q}\right)\times\prod_{j=1}^{3N-6}\pi^{-1/4}2^{n_j}n_j!\Gamma_j^{1/4}H_{n_j}(\Gamma_j^{1/2}Q_j) \tag{3.6}$$

where $\mathbf{Q}$ is the column vector of the normal coordinates, $\mathbf{\Gamma}$ is the diagonal matrix of the reduced frequencies (Γ_j=$\omega_j/\hbar$), and H_j is the jth Hermite polynomial.

In the case of an electronic transition, initial- and final-state normal coordinates are related by the transformation:

$$\mathbf{Q}_f=\mathbf{J}\mathbf{Q}_i+\mathbf{K} \tag{3.7}$$

where $\mathbf{J}$ is the Duschinsky matrix and the vector $\mathbf{K}$ expresses the geometry change in the final state. The $\mathbf{J}$ matrix reflects the mapping of the normal modes of the initial-state system onto those of the final-state system. A considerable simplification is introduced by assuming that the off-diagonal elements in $\mathbf{J}$ are very small. In this case, the intensity of transition is given by a product of one-dimensional Franck-Condon factors, see (Ansbacher 1959). In the one-dimensional case, the Ansbacher recurrence relations for Franck-Condon integrals are

$$I(0,0) = \sqrt{\frac{2\beta}{1+\beta^2}}\,exp\left[-\frac{1}{2}(\Gamma_f^{1/2}K)^2\frac{\beta^2}{1+\beta^2}\right] \tag{3.8}$$

$$I(0,1) = (\Gamma_f^{1/2}K)\frac{\beta^2}{1+\beta^2}\sqrt{2}\,I(0,0) \tag{3.9}$$

$$I(n>1) = (\Gamma_f^{1/2}K)\frac{\beta^2}{1+\beta^2}\sqrt{\frac{2}{n}}I(0,n-1)+\frac{1-\beta^2}{1+\beta^2}\sqrt{\frac{n-1}{n}}I(0,n-2) \tag{3.10}$$

where $(\Gamma_f^{1/2}K)$ is the displacement in final-state reduced coordinates, and β=Γ_i/Γ_f.

Vibrational structure in XPS of clusters

The vibrational structure in a core-level XPS of a cluster can be separated into intra- and inter-molecular components. The intramolecular contribution is taken to be similar to that of the free monomer, whereas the contribution of intermolecular vibrations can be represented by a Gaussian distribution with a width (Cederbaum and Domcke 1976, Thomas et al. 1998)

$$\sigma = 2ln(2)\sqrt{\sum_j \left(\frac{\partial E}{\partial Q_j}\right)^2 \Gamma_j^{-1}} \tag{3.11}$$

where $\left(\frac{\partial E}{\partial Q}\right)$ is the projection of the final state forces on the displacement vectors of the mass-weighted normal coordinates of the initial state.

3.1.3 Other information in XPS

Spin-orbit coupling

Photoionization often leads to final states with non-zero spin. In particular, this applies to the most common case of photoelectron transitions from a neutral ground state that is a singlet state. In the final state, the total spin is coupled to the orbital angular momentum and if this is non-zero we will obtain two different states, depending on whether the spin angular momentum is aligned parallel or anti-parallel to the orbital angular momentum. The strength of the spin-orbit coupling depends primarily on the distance of the electron from the nucleus. The spin-orbit coupling gives rise to peak splitting in photoelectron spectra.

Molecular field splitting

Molecular field splitting (MFS) has been observed in photoelectron spectra of inner-shells with angular momenta greater than zero (Svensson et al. 1994). The mechanism of splitting has been identified as asymmetry in the electric field about the probed nucleus. The MFS gives rise to either peak splitting or extra broadening, depending on the width of the peak in question.

Partial localization of core electrons

Core levels have always been regarded as essentially atomic in character. However, recent studies have revealed that equivalent atoms with very short internuclear distance and degenerate core orbitals, e.g. carbon atoms in acetylene, form symmetric and

asymmetric linear combinations of their 1s orbitals (Kempgens et al. 1997). The core-hole states of such a molecule occur in pairs of nearly degenerate states of $gerade$ and $ungerade$ symmetry, with $gerade$-$ungerade$ energy splitting very sensitive to the internuclear distance. In the case of acetylene where the CC bond distance is 1.2 Å, the core-level energy splitting is of order of 100 meV.

3.2 Line broadening mechanisms

The observed spectrum is a convolution of the vibrational structure, the intrinsic lineshape, and the experimental resolution. The experimental resolution is represented by a Gaussian distribution with a width determined by the monochromator slit and the spectrometer settings, see chapter 2. The intrinsic lineshape depends on the lifetime of the excited state and the effect of post-collision interactions (PCI). These two phenomena are discussed in the following subsections.

3.2.1 Lifetime broadening

By emitting a core electron, the system makes a transition to a state of finite lifetime τ. From Heisenberg uncertainty principle, any state that has a finite lifetime must be regarded as having an imprecise energy. This gives rise to lifetime broadening of spectral lines. Lifetime broadening transforms the discrete vibronic transitions into Lorentzian functions of the form

$$I(\epsilon) = \frac{\text{Constant}}{\left((E_0 - h\nu) + \epsilon\right)^2 + \frac{\Gamma^2}{4}} \tag{3.12}$$

Here, ϵ is the kinetic energy of photoelectrons, 'Constant' refers to terms that are slowly varying over the energy range of interest, $\Gamma = \hbar/\tau$, and E_0 is the nominal ionization energy. The Lorentzian function is characterized by a long tail which considerably reduces the contrast and the possibility to separate and identify the fine structural features.

Theoretical calculations indicate that the lifetime for a core hole in a free atom is longer than that of the same atom in a molecule. Moreover, the core hole is, to some extent, sensitive to the chemical composition of the molecule. For example, the calculated lifetime for carbon 1s hole in CH_4 is found to be longer than that in CF_4. (Hartmann 1988)

3.2.2 Post-collision interactions

Core holes may decay by Auger electron or x-ray emission. Auger process dominates for light elements. If Auger decay occurs and if the energy of the Auger electron, ϵ_A, is

greater than the kinetic energy of the photoelectron, ϵ, the Auger electron will overcome the photoelectron and change its energy to $\acute{\epsilon} = \epsilon - \delta$. Since the total energy is conserved, the energy of the Auger electron becomes $\acute{\epsilon}_A = \epsilon_A + \delta$.

The general expression that gives the lineshape function where lifetime broadening and post-collision interactions (PCI) are included is

$$I(\acute{\epsilon}, \epsilon) = \frac{\Gamma}{2\pi} \frac{1}{\frac{1}{4}\Gamma^2 + (\acute{\epsilon} - \epsilon)^2} \frac{\pi C \exp\left[2(C/\nu_1)\arctan(2(\acute{\epsilon} - \epsilon)/\Gamma)\right]}{\nu_1 \sinh(\pi C/\nu_1)} \tag{3.13}$$

where ν_1 is the velocity of the photoelectron, and C is an angular dependence parameters. In ref. (van der Straten et al. 1988), C is given for isotropic emission as $1 - (\epsilon/\epsilon_A)^{1/2}$. In atomic units ν_1 is $(2\epsilon)^{1/2}$. Then C/ν_1 becomes $2^{-1/2}(\epsilon^{-1/2} - \epsilon_A^{-1/2})$, with energies given in atomic units.

Recent studies on noble gas clusters report that atoms in the bulk phase are observed to be less affected by post collision interaction than atoms at the cluster surface. (Lindblad et al. 2005)

3.3 Lineshape models

3.3.1 Free atoms

The XPS lineshape of a free atom is just a convolution from a Lorentzian distribution that accounts for the lifetime broadening, a Gaussian distribution that represents the instrumental resolution, and a PCI function.

3.3.2 Free molecules

Modeling an inner-shell photoelectron spectrum of a free molecule is more complicated than it is for a free atom. It involves calculations of vibrational excitations. The molecular lineshape is thus a convolution of the vibrational structure with broadening functions that reflect the natural linewidth, the instrumental resolution, and post-collision interactions.

In some cases,i.e. CH stretching mode in methane, including anharmonicity effects in the calculations of vibrational excitations produces much better agreement with experiment (Carroll et al. 1999).

3.3.3 Clusters

The lineshape associated with ionization of a single monomer in a cluster is taken to be similar to that of the free monomer, only shifted in ionization energy according to the

position of the monomer in the cluster. Changes to the vibrational envelope induced by the cluster environment are modeled by a Gaussian distribution with a width given by eq. 3.11. Thus, the cluster spectrum is regarded as a sum of monomeric Franck-Condon profiles that are displaced in energy based on the distribution of ionization energies pertaining to the cluster, and convoluted with a Gaussian distribution that represents intermolecular vibrational broadening.

Chapter 4

Theoretical and Computational Models

In this chapter we present a number of concepts and techniques that are relevant to our work. We start with the Born-Oppenheimer approximation, where the motion of the electrons is decoupled from the motion of the nuclei. In sections 4.2 and 4.3, we show the potential energy functional forms and computer simulation methods employed in our study of clusters. The electronic structure problem is presented in section 4.4.

4.1 The Schrödinger equation

In theoretical chemistry we aim to find approximate solution to the time-independent Schrödinger equation

$$H\Psi\left(\mathbf{R},\mathbf{r}\right)=E\Psi\left(\mathbf{R},\mathbf{r}\right) \tag{4.1}$$

where H is the Hamiltonian operator, $\Psi\left(\mathbf{R},\mathbf{r}\right)$ is the total wavefunction, $\mathbf{r}$ is the electronic coordinate vector and $\mathbf{R}$ is the nuclear coordinate vector. The Hamiltonian for a system of N nuclei and M electrons is given in atomic units as (Szabo and Ostlund 1989)

$$H=-\sum_{i=1}^{M}\frac{1}{2}\nabla_i^2-\sum_{A=1}^{N}\frac{1}{2m_A}\nabla_A^2-\sum_{i=1}^{M}\sum_{A=1}^{N}\frac{Z_A}{r_{iA}}+\sum_{i=1}^{M}\sum_{j>i}^{M}\frac{1}{r_{ij}}+\sum_{A=1}^{N}\sum_{B>A}^{N}\frac{Z_AZ_B}{R_{AB}} \tag{4.2}$$

where m_A is the mass of nucleus A, and Z_A is its atomic number. The first and the second terms in Eq. 4.2 are the operators for the kinetic energy of the electrons and of the nuclei, respectively. The third term represents the coulomb attraction between electrons and nuclei, and the fourth and fifth terms represent the repulsion between electrons and between nuclei, respectively.

4.1.1 Born-Oppenheimer approximation

Since the nuclei are much heavier, and therefore slower, than the electrons one can consider the electrons to be moving in the field of fixed nuclei. This approximation is commonly known as the Born-Oppenheimer approximation. Within this approximation,

the molecular Hamiltonian can be splitted into a nuclear part and an electronic part. The corresponding approximation to the total wavefunction is

$$\Psi(\mathbf{R}, \mathbf{r}) = \phi(\mathbf{r}; \mathbf{R})\, \psi(\mathbf{R}) \tag{4.3}$$

where $\phi(\mathbf{r}; \mathbf{R})$ is the electronic wavefunction and $\psi(\mathbf{R})$ is the nuclear wavefunction.

4.2 Classical mechanics

In cartesian space, the position of a system of N particles is defined by a vector $\mathbf{R}$ where

$$\mathbf{R} = (x_1, y_1, z_1, \ldots, x_N, y_N, z_N) \tag{4.4}$$

and x_i, y_i, and z_i are the coordinates of particle i. The Hamiltonian for this system is

$$H = T + U \tag{4.5}$$

where T is the kinetic energy and U is the potential energy. The potential energy due to classical particle-particle interactions is broken into different components:

$$U = U_{val} + U_{vdW} + U_{coul} \tag{4.6}$$

where U_{val} is the energy due to valence interactions, U_{vdW} is the energy due to van der Waal interactions, and U_{coul} is the energy due to electrostatic interactions. Non-bonded interactions, both van der Waals and electrostatic, play important role in determining the structure of molecular species.

In our work on clusters, we use a force-field approach in the calculations of chemical shifts in core-level ionization energies, and vibrational broadening due to excitation of intermolecular modes. The force field is developed by a group in the USA and is given the name AMOEBA (Ren and Ponder 2003, Ren and Ponder 2002). AMOEBA uses a polarizable-atomic-multipole description of electrostatic interactions. This feature is very important when probing the response of chemical surroundings to a positive charge.

Now we will consider the functional forms of the AMOEBA force field.

Valence energy

The valence interactions represent bond stretching, angle bending, internal torsion, in addition to improper torsion and out-of-plane bendings. The improper torsion and out-of-plane bending are not significant to our study, hence, they will be omitted. The general forms for bond stretching and angle bending terms are Taylor expansions of

Morse potential through the fourth power and the sixth power, respectively. The general form for bond-stretching energy is

$$U_{str} = \frac{k_{str}}{2}(R - R_0)^2 \left[1 - k_R^{'}(R - R_0) - k_R^{''}(R - R_0)^2\right] \tag{4.7}$$

where k_{str} is the bond-stretching force constant, and R_0 is the minimum-energy bond distance. The force field employs cross terms (Allinger et al. 1989). The stretch-bend cross term reads

$$U_{cross} = \frac{k_{cross}}{2}\left[(R - R_0) + (\acute{R} - \acute{R}_0)\right](\theta - \theta_0). \tag{4.8}$$

This term allows the bonds R and $\acute{R}$ to stretch out when the angle θ between them is reduced. Other cross terms, i.e. stretching-torsion and bending-torsion, will not discussed here because they are not significant to our study.

The torsion itself is periodic. Therefore, the functional form of the torsional energy must be periodic too. The torsional energy is well represented by Fourier series expansion (Allinger et al. 1989)

$$U_{tors} = \frac{1}{2}\sum_k V_k\,(1 - kcos(\omega)) \tag{4.9}$$

where ω is the torsional angle, and V_k gives qualitative indication of the relative barriers to rotation.

vdW energy

The pairwise vdW interactions are modeled by a buffered 14-7 potential (Halgren 1992) with the following functional form

$$U_{vdW}^{ij} = \epsilon_{ij}\left(\frac{1+\delta}{\rho_{ij}+\delta}\right)^{n-m}\left(\frac{1+\gamma}{\rho_{ij}^m+\gamma} - 2\right) \tag{4.10}$$

where ϵ_{ij} is the potential well depth, $\rho_{ij} = R_{ij}/R_{ij}^*$ with R_{ij} as the i-j distance and R_{ij}^* is the minimum-energy distance. Fixed values of n=14, m=7, δ=0.07, and γ=0.12 are applied in this force field.

Electrostatic energy

The electrostatic interactions are divided into two main categories: permanent multipole interactions and polarization interactions. Components of the permanent multipoles up to the quadrupole moments are evaluated for each atomic site by means of distributed multipole analysis (Stone 1981, Stone 2005). These multipoles must be

transformed into a local-coordinate frame before being employed in AMOEBA force field (Ren and Ponder 2003). The atomic multipole row vector M reads

$$M = \left[\begin{array}{ccccccc} q & \mu_x & \mu_y & \mu_z & Q_{xx} & \ldots & Q_{zz} \end{array} \right] \tag{4.11}$$

where q is the atomic charge, μ is the atomic dipole, and Q is the atomic quadrupole.

The intramolecular polarization interactions are group-based as a means of merging the polarization model with local valence terms. The polarization effects are explicitly treated via direct induction of permanent multipoles and mutual induction of induced atomic dipoles. Short range interactions are damped in order to avoid polarization catastrophe. The induced dipoles are computed as

$$\mu_{i,a}^{ind} = \alpha_i \left(\sum_j T_a^{ij} M_j + \sum_{j'} T_{ab}^{ij'} \mu_{j,b}^{ind} \right) \tag{4.12}$$

where α_i is the polarizability of atom i, T_a^{ij} is the interaction matrix between site i and site j, a and b are indices to the xyz-components of the induced dipole and the interaction matrix. The first sum in Eq. 4.12 corresponds to induction due to the permanent multipoles, the sum runs over all atoms outside the polarization group of atom i. The second sum in Eq. 4.12 corresponds to the induction caused by induced dipoles at all sites other than i.

4.3 Molecular Dynamics simulations

Computer simulations enable us to study large systems, determine their time-dependent behavior, and predict their properties. In this section we present the basics of one of the most common techniques used in molecular modeling: Molecular Dynamics (MD).

The differential equation

$$\frac{d}{dt} \left(\frac{\partial H}{\partial \dot{R}_i} \right) + \frac{\partial H}{\partial R_i} = 0 \tag{4.13}$$

gives the relation between accelerations, velocities, and coordinates. It constitutes a set of second-order differential equations in **R**, which can be solved if the state of the system is specified at some given instant. For example, if the coordinates **R** and the velocities $\dot{\mathbf{R}}$ are specified for a system at time t, then its acceleration $\ddot{\mathbf{R}}$ is uniquely defined and its subsequent motion can be calculated. This gives rise to an important concept in computer simulations, that is, for a system of N particles, 3N coordinates and 3N velocities are required to define the state of the system.

Substituting Eq. 4.5 in Eq. 4.13 gives

$$m_i \frac{d\dot{R}_i}{dt} = -\frac{\partial U}{\partial R_i} \tag{4.14}$$

where $\frac{\partial U}{\partial R}$ is the force on the ith particle, and m_i is its mass. This is Newton's second law of motion. This equation shows how the acceleration and the coordinates of the particles vary with time. In molecular dynamics, the development of the system trajectory with time can be obtained by integrating the Newton's equation of motion. Since the potential energy depends on the positions of the particles, any small perturbation in the position of any particle instantaneously affects all other particles. Under such circumstances, the equations of motion are integrated using finite difference methods.

The basic idea of finite difference is to break the integration into many small steps, with a fixed time difference of δt. There are different algorithms for doing the integration, i.e Verlet, *leap-frog*, and Beeman. (Leach 2001) All of them assume that the coordinates, the velocities, and the accelerations can be approximated by Taylor series expansions. In our study, the trajectories are propagated using the Beeman algorithm as modified by Brooks (Beeman 1976, Brooks 1988). The following equations show the integration scheme in $\mathbf{R}$ and $\dot{\mathbf{R}}$.

$$\mathbf{R}(t+\delta t) = \mathbf{R}(t) + \delta t\dot{\mathbf{R}}(t) + \left[5\ddot{\mathbf{R}}(t) - \ddot{\mathbf{R}}(t-\delta t)\right]\frac{\delta t^2}{8} \tag{4.15}$$

$$\dot{\mathbf{R}}(t+\delta t) = \dot{\mathbf{R}}(t) + \left[3\ddot{\mathbf{R}}(t+\delta t) + 6\ddot{\mathbf{R}}(t) - \ddot{\mathbf{R}}(t-\delta t)\right]\frac{\delta t}{8} \tag{4.16}$$

4.4 Electronic-structure calculations

We aim to calculate accurate electronic structures of neutral and core-ionized molecules. Among several methods, density functional theory is shown to be the most cost-effective method to achieve a given level of accuracy. (Parr and Yang 1989)

4.4.1 Density functional theory

The history of density functional theory (DFT) begins with the work of Thomas and Fermi in 1920's. The key theories of DFT were presented by Hohenberg and Kohn in the 1960's. The basic idea of DFT is that knowing the electron density is all that is necessary for a complete determination of the wavefunction and the energy of the molecule.

The energy of a molecule can be given as a functional of the electron probability density ρ,

$$E[\rho] = T[\rho] + V_{ne}[\rho] + V_{ee}[\rho] \tag{4.17}$$

where $T[\rho]$ is the kinetic energy, $V_{ne}[\rho]$ represents the attraction between electrons and nuclei, and

$$V_{ee}[\rho] = J[\rho] + E_{xc}[\rho] \tag{4.18}$$

where $J[\rho]$ is a classical electron-electron repulsion term, and $E_{xc}[\rho]$ is a non-classical exchange-correlation term. Several density functionals have been developed to describe $E_{xc}[\rho]$, i.e. LSDA, BLYP and B3LYP. (Cramer 2002, Stephens et al. 1994) In our work we have used the B3LYP functional. This functional is a hybrid of exact Hartree-Fock (HF) exchange with local and gradient-corrected exchange and correlation terms (Stephens et al. 1994)

$$E_{xc}^{\text{B3LYP}} = (1-a)E_x^{\text{LSDA}} + aE_x^{\text{HF}} + b\Delta E_x^{\text{B}} + (1-c)E_c^{\text{LSDA}} + cE_c^{\text{LYP}} \tag{4.19}$$

Here, a, b, and c are semi-empirical coefficients optimized to 0.20, 0.72, and 0.81, respectively, E_x^{LSDA} and E_c^{LSDA} are the exchange and correlation functionals from LSDA, E_x^{HF} is the exact HF exchange, ΔE_x^{B} is Becke's gradient correction to the exchange functional (Becke 1993), and E_c^{LYP} is LYP gradient correction to the correlation functional. (Lee et al. 1988)

4.4.2 Description of core-hole states

Electronic-structure calculations for a species with a core hole are far from simple. This has led to popularity of the equivalent-core method which circumvents the difficulties encountered in the direct-hole method by replacing the exact calculation of the hole state with a ground-state calculation of the equivalent system with a (Z+1) charge on the nucleus of the atom in question (e.g. C(1s)$^{-1}$ is replaced by N). This approximation has an intrinsic error when used for computing geometries and vibrational frequencies of core-ionized molecules. (Thomas et al. 1998, Karlsen and Børve 2000) In this work we use an effective-core potential (ECP) to simulate the ionized core. (Stevens et al. 1984) The effective-core potentials are usually presented as a linear combination of functions of the type $r^{-n}\exp[-\alpha r^2]$ whose coefficients and exponents are determined by least-squares fits to numerical tabulations of the potentials. The prospects of using ECP in the calculations of vibrational structures in inner-shell photoelectron spectra have been investigated and found to be satisfactory. (Karlsen and Børve 2000)

Chapter 5

Carbon 1s Photoelectron Spectra of Ethanol

In this chapter we shed light on a very new topic, that is, conformational effects in inner-shell photoelectron spectra of gas-phase molecules. The question to be answered is whether different molecular conformations would display different core-level spectra or not. This question has been addressed in a recent study on carbon 1s photoelectron spectra of butan-2-ol, and no such effects were observed (Rennie et al. 2002). On the contrary, we found experimental and theoretical evidences that show just such effects in the carbon 1s photoelectron spectrum of ethanol. The theory development that led to this result is presented in papers I and II.

Ethanol shows two stable conformations that interconvert by torsion of the hydroxyl group: *anti* and *gauche* (Senent et al. 2000, Shaw et al. 1989, Kaker and Quade 1980). Figure 5.1 shows the torsional potentials for both neutral and core-ionized ethanol, as obtained from B3LYP calculations. While all three curves show minima at the *anti* conformation, minima at the *gauche* conformation are present only in neutral ethanol and ethanol that is core-ionized at the functionalized carbon. This implies that ionization at the methyl carbon takes the gauche conformation to a repulsive final-state energy curve. The geometry relaxations accompanying this transition are extreme, and the corresponding XPS lineshape becomes broad and featureless. Conversely, ionization of the *anti* conformation leads to a well-structured lineshape.

After giving a detailed analysis, we found that the vibrational profile resulting when the *gauche* conformation is ionized at the methyl carbon arises from extreme excitation of the HOCC torsional mode, and additionally, from anharmonic coupling of this mode to other modes. Indeed, this is one of the cases where the harmonic approximation breaks down both at the single and multi-mode levels. Hence, we have to calculate Franck-Condon factors taking into accounts anharmonicity effects.

To take mode coupling into account, we augment the final-state potential energy surface by binary coupling terms between the HOCC mode, labeled z_1, and mode *k*, as

$$W_k(z_1, q_k) = A_k(z_1)q_k + B_k(z_1)q_k^2 \tag{5.1}$$

Here, A_k and B_k are polynomials in z_1, the coefficients of which are determined from a grid in z_1 and q_k. Based on an algorithm developed in paper II, four modes were found

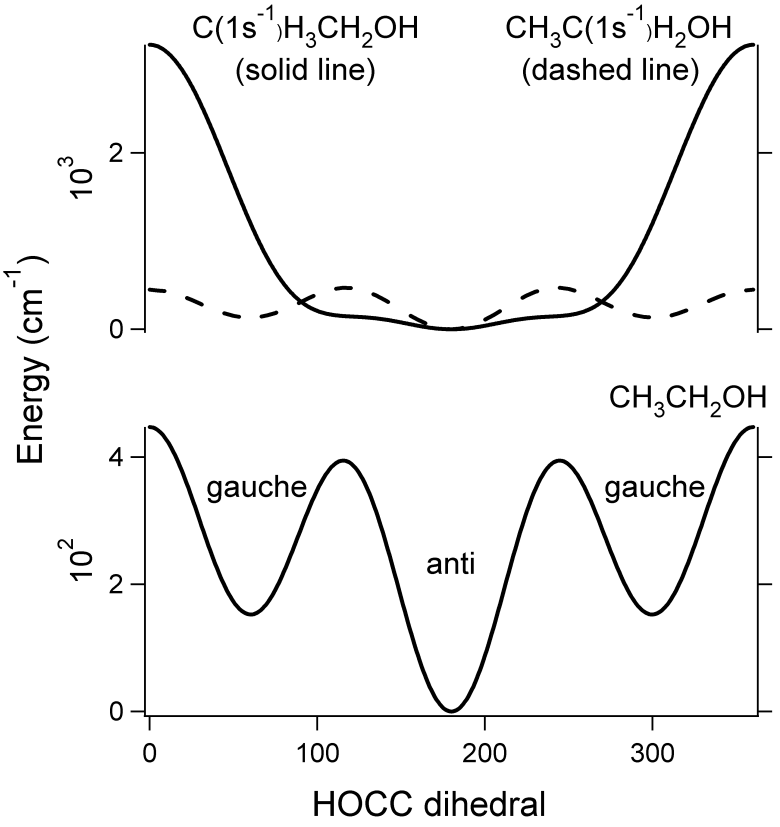

Figure 5.1: *Theoretical potential energy curves for torsion about the OC bond. Top curves: Ethanol core ionized either at the methyl end (solid line) or at the functionalized end (dashed line); Bottom: Neutral ethanol.*

to couple sufficiently strongly to the HOCC mode. These are methyl torsion, CCO bending, a combination mode dominated by HOC and CCH bending, and CO stretching. For coupling of z_1 to the methyl torsion, which is particularly strong, W_k is taken to fifth order in both of the normal coordinates. To facilitate this within the present formalism, we included the methyl torsion in the set of highly-excited anharmonic oscillators as z_2. The Hamiltonian of the coupled modes reads

$$H = H_z + \hbar^2 \sum_{k=1}^{3} \Gamma_k \left(n_k + \frac{1}{2} \right) + \hbar^2 \sum_{k=1}^{3} \Gamma_k \left[A_k(z_1) q_k + B_k(z_1) q_k^2 \right] \tag{5.2}$$

where $H_z = H_{z_1} + H_{z_2} + W(z_1, z_2)$, and $\Gamma_k = \frac{\omega_k}{\hbar}$. If we were dealing with one or two degrees of freedom, then the simplest way to solve the system would be to diagonalize a matrix representation of the Hamiltonian in a basis set. This has been done before, but no so for systems with more than three degrees of freedom (Tromp and Miller 1986, Luis et al. 2004). This is because basis sets for molecular problems typically require 10-20 basis functions per degree of freedom. So, what do we do?

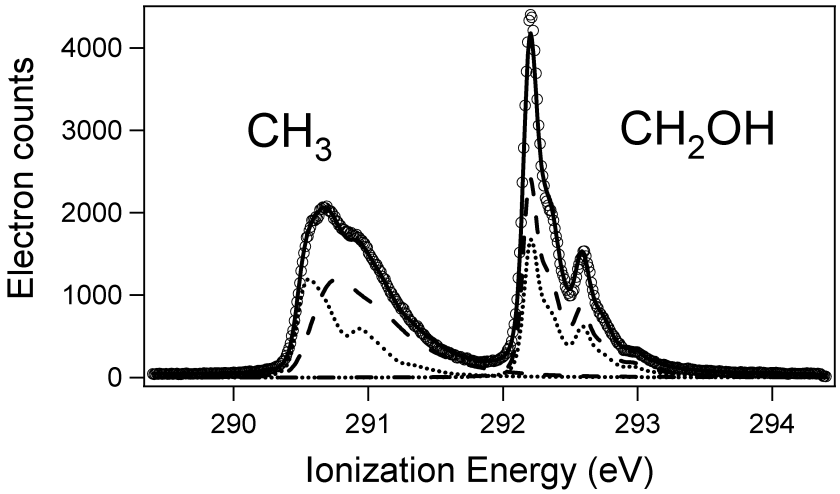

Figure 5.2: *Experimental (circles) and theoretical (solid line) carbon 1s photoelectron spectrum of ethanol. The individual contributions from the anti (dotted lines) and the gauche (dashed lines) conformations are also shown.*

We made use of the reaction path Hamiltonian theory, and more precisely, the basis set method advocated by Makri and Miller for describing a one-dimensional reaction coordinate coupled to a bath of many harmonic oscillators (Miller et al. 1980, Makri and Miller 1987). Within this approach, the model of a few highly-excited modes coupled to a bath of harmonic modes is treated by eliminating all the harmonic modes. When this approach is applied to the present case, eq. 5.2 becomes

$$H = H_z + \hbar^2 \sum_{k=1}^{3} \acute{\Gamma}_k \left(n_k + \frac{1}{2} \right) - \frac{1}{2} \hbar^2 \sum_{k=1}^{3} \Gamma_k \frac{A_k^2}{1 + 2B_k} \tag{5.3}$$

where $\acute{\Gamma} = \Gamma(1 + 2B)^{1/2}$. In comparison with eq. 5.2, mode coupling is now expressed only in terms of z_1. The most powerful feature of this approach is that the treatment of the harmonic oscillators will be based on simple analytical expressions, so that one is left with an effective Hamiltonian, the matrix representation of which can be diagonalized in a small basis set. It should be emphasized, though, that mode coupling is not entirely included in the effective Hamiltonian (in eq. 5.3). It enters also via the Franck-Condon integrals, which are defined as

$$I_{\mathbf{n}i} = \int \psi_{\mathbf{n}i}(z_1) \left[\prod_{k=1}^{3} I_{n_k}(z_1) \right] \psi_{init}(z_1) dZ_1. \tag{5.4}$$

In cases when $I_{n_k}(z_1)$ varies only slowly with z_1, the Franck-Condon integrals may be factorized into k and z contributions. The results of this approach are tested against

previous exact results obtained by means of eq. 5.2 and the agreement between the two methods is excellent. This approach has been adopted in the calculations of the lineshape of *gauche*-ethanol core ionized at the methyl carbon.

The carbon 1s photoelectron spectrum of ethanol is shown in Fig. 5.2. We found significant mismatch between the observed XPS spectrum and theoretical lineshape models based on any single molecular conformation. On the other hand, a theoretical lineshape composed out of 60% *gauche*- and 40% *anti* profiles provides excellent fits to the observed spectrum. In light of this result, we anticipate this phenomenon to be common in inner-shell photoelectron spectra of molecules that exhibit conformational equilibria. But in order to observe it, the conformations must be present in comparable amounts in the ground state, and core ionization of at least one site must lead to different vibrational profiles for the different conformations.

Chapter 6

XPS Lineshape Models of Clusters

Clusters are aggregates of atoms or molecules. They are formed by most of the elements of the Periodic Table, and the types of bonding and the resulting clusters are equally varied. Clusters range in size from small oligomers to many millions, thereby bridging the gap between the small molecules and bulk materials. One of the most compelling reasons for studying clusters is the size-dependent evolution of their physical and chemical properties. Nowadays, there is considerable experimental and theoretical research with the aim of tuning properties to desired values by selection of clusters of suitable size. Examples of present and future applications of clusters include the use of clusters as components of nanodevices, the use of clusters deposited on surfaces for heterogeneous catalysis, and the construction of novel materials, where the building blocks are clusters rather than individual atoms or molecules (Johnston 2002, Attfield et al. 1999, Schmid 1999).

Clusters may be classified according to the type of building units and the nature of bonding into metallic, covalent, ionic, rare-gas, and molecular clusters. Both rare-gas and molecular clusters are of particular interest to our research group. Rare-gas clusters make useful model systems for detailed studies of surface effects. Indeed, they allow the investigation of interfaces with a shell-like geometric structure (von Pietrowski et al. 2006). Regarding molecular clusters, they form a sensitive testing ground for our understanding of intermolecular interactions at interfaces, in the bulk and in the transition zone between these.

In the past years, most of the studies performed on clusters have mainly applied comparatively simple experimental techniques, such as mass abundance spectroscopy and ionization energy studies. The results obtained from these techniques, though, were not sufficient for detailed understanding of electronic and geometric structures of clusters. Hence, it has been necessary to apply more sophisticated experimental techniques to cluster studies. This led to the popularity of electron spectroscopy which allows the exploration of both specific and smooth structural changes, and electronic and dynamic cluster-size effects. However, electronic spectra of molecular clusters show great complexity, depending on the experimental technique employed. To reduce the complexity of the spectra, we will be concerned with the technique of core-level x-ray photoelectron spectroscopy (XPS).

Core-level XPS highly discriminates between different atomic sites, e.g. between bulk and surface atoms. It is also sensitive to the variations in surface geometry and coordination. We make use of the local-probing property of core-level XPS in the investigations of atomic and molecular clusters. Information of primary interest concerns chemical shifts between bulk and surface monomers, which may be used to gain insight into the local surrounding of the ionized atom, and hence the intermolecular geometry. However, it is often the case that core-level photoelectron spectra are broad and featureless, so the chemical shift in question may be hard to obtain. Thus, it is useful to compare the experimental spectra to theoretical lineshape models that represent well-defined bonding regimes in the cluster. Our work on the development of theoretical methods for modeling and analyzing inner-shell photoelectron spectra of rare-gas and molecular clusters is presented in papers III to V. In this chapter we will present the major results, and discuss each of them briefly.

Main results

XPS and the size of neutral Ar clusters

Rare-gas clusters are formed in a supersonic beam expansion. The experimental setup developed for this purpose is described elsewhere (Tchaplyguine et al. 2003). The expansion gives a distribution of clusters, with a mean size can be varied by changing the expansion conditions. Rare-gas clusters of size up to several hundreds of atoms favor icosahedral geometric shells, whereas those of larger size favor cuboctahedral geometric shells. This has been explained as follows: in icosahedral structures the surface contacts are longer than the radial contacts. For small sizes, minimizing the surface energy outweighs the effect of shortened radial distances. However, as the size increases bulk compression becomes larger and larger, which eventually destabilizes the icosahedral structures relative to the cuboctahedral structures (Johnston 2002). The transition from icosahedral- to cuboctahedral structure has been a subject of interest and debate in many publications (Farges et al. 1983, Lee and Stein 1987, Kakar et al. 1997).

A typical core-level photoelectron spectrum of a rare-gas cluster is shown in Fig. 6.1. This specific spectrum shows the $2p_{3/2}$ XPS lineshape of argon clusters. It is obvious that core-level XPS is able to distinguish between bulk and surface monomers. The main mechanism that ensures this is the increased electronic relaxation that benefits the bulk monomers as compared to those in the surface layer (Björneholm et al. 1995, Björneholm et al. 1996). It follows that rare-gas clusters serve as good role models to map the development of properties from atomic to bulk materials, i.e. by monitoring the size-dependent evolution of bulk- and surface properties. But so far it has been

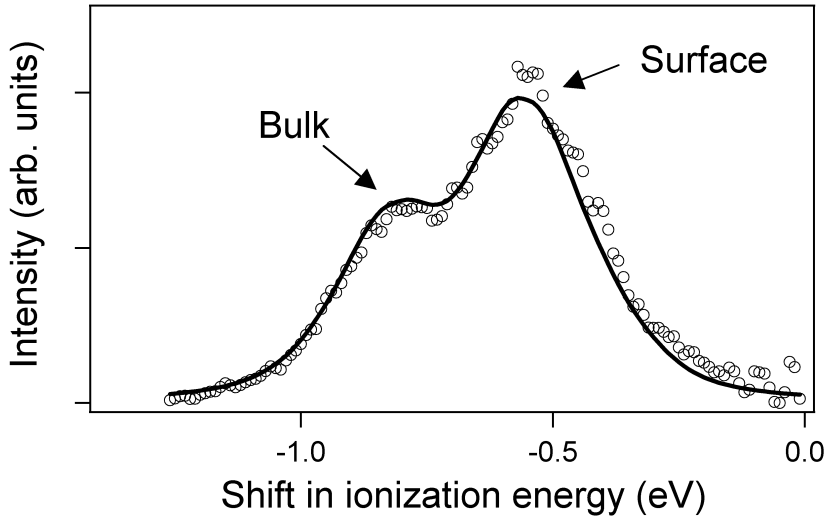

Figure 6.1: *Experimental (circles) $Ar2p_{3/2}$ photoelectron spectrum corresponding to small clusters fitted with a theoretical lineshape (solid line). The ionization energy is given relative to that of the free atom.*

difficult to take this correlation beyond the qualitative level, as it is very difficult to ascertain the size distribution of neutral clusters.

The determination of cluster sizes, especially for neutral clusters which are not mass selected, is far from simple. Several experimental approaches have been applied to solve this fundamental problem (Hagena 1987, Buck and Krohne 1996, Karnbach et al. 1993, Farges et al. 1986). Still, the important issue characterizing jet expansions that lead to cluster formation is not fully solved. This has motivated us to present another approach to determining the size of neutral rare-gas clusters from photoelectron spectra. By fitting theoretical lineshapes to photoelectron spectra of rare-gas clusters, one may have a reasonably robust way of determining the actual cluster size.

A common approach to modeling XPS spectra of rare-gas clusters is to fit the cluster band by two monomer spectra displaced in energy and further broadened by Gaussian distributions, which represent the contributions from bulk and surface environments. This approach provides good fits to the experimental spectra, and useful information concerning ionization energies and linewidths of both bulk and surface fractions can be obtained. However, it does not provide insight into the size-distribution of rare-gas clusters.

A more adequate approach is one where a quantitative model that takes into account all known contributions to the lineshape is used. In this model, the cluster lineshape is regarded as a sum of monomer spectra which are displaced in energy according to the distribution of ionization energies in the cluster, and further convoluted by the vibrational excitations of normal modes. The lineshape accounts also for the attenuation of

the signal intensity (Tchaplyguine et al. 2004).

We used this approach in the calculations of lineshape models for argon clusters. The spectrum (in fig. 6.1) pertains to argon clusters with a mean size in the range where icosahedral structures are dominant. Hence, we focus on clusters with icosahedral structures. We compute lineshape models for icosahedral clusters with both open- and closed outermost geometric shells. The geometries of the closed-shell clusters are constructed according to (Xue 1993). Regarding clusters with open geometric shells, we found that atoms in the surface layer are most likely to form one large island instead of several smaller ones.

The chemical shift is calculated by means of a polarizable electrostatic model, where a positive charge is placed at a specific site in the cluster and is allowed to interact with the induced dipoles of the surrounding atoms (Björneholm et al. 1996, Stampfli 1995). Our calculations indicate that the main contributors to charge screening are the atoms in the first geometric shell around the positive charge. Thus, atoms with lower number of nearest neighbors are less screened, and their spectral signal is predicted at higher ionization energies. This supports the above interpretation of the experimental spectra as being composed of surface and bulk contributions.

The vibrational broadening due to excitations of normal modes can be modeled by a Gaussian distribution with a width obtained from the projection of final-state forces, calculated in the vertical geometry, on the neutral-cluster normal modes of vibration (Cederbaum and Domcke 1976, Thomas et al. 1998). The calculations have shown that line broadening due to excitations of cluster modes is negligible for both bulk and surface atoms.

We account for the lost signal due to inelastic scattering of photoelectrons by including an exponentially decaying scattering expression over the geometry of the cluster. This expression is very sensitive to the choice of the effective escape depth (λ). This is the distance photoelectrons can travel before they get scattered. By comparing theoretical lineshape models, computed with different values of λ, to the experimental spectra, we came up with an estimate range of $10 \leq \lambda \leq 15$ Å. Our results are in agreement with the values reported in the literature (Amar et al. 2005, Tchaplyguine et al. 2004, Tanuma et al. 1994)

Since the experimental spectra pertain to a distribution of cluster sizes, it is convenient to incorporate this feature in the theoretical spectra, by adopting an analytical model for the size distribution. We have used the log-normal distribution function, because it has been able to explain the size distribution of nanoparticles made with the gas evaporation technique (Kiss et al. 1999). In order to explore the sensitivity of the log-normal function, the results are compared to those obtained for Poisson and normal functions, and the agreement is satisfactory.

The spectrum in fig. 6.1 is fitted with calculated lineshapes, assuming a log-normal

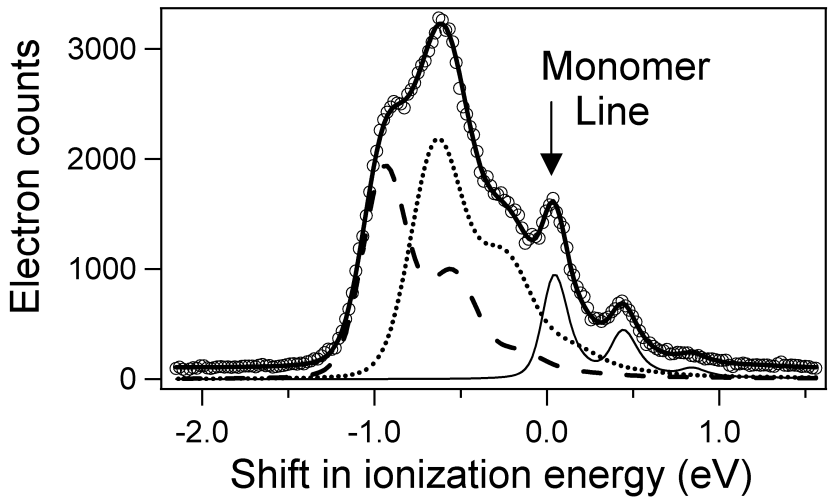

Figure 6.2: *Carbon 1s photoelectron spectra of methane clusters and free monomers. Experimental data are shown as circles and lines are used to represent fitting models. The thin solid line at higher ionization energy represents uncondensed methane molecules; the dotted line represents methane molecules in the surface layer of a cluster; the dashed line represents methane molecules in the bulk of a cluster; and a thicker solid line shows the full model spectrum.*

size-distribution function and λ =15 Å. The mean cluster size estimated from the simulated spectra is about a factor of two higher than the gas-dynamic estimations using the Hagena laws (Hagena 1987). This indicates that the size estimators from expansion conditions may underestimate the mean cluster size. This result has been supported by other reports (Tchaplyguine et al. 2004).

The evolution of XPS from atomic to molecular clusters

While core-level photoelectron spectra of rare-gas clusters display well-resolved surface and bulk features, see for instance fig 6.1, the situation may be more complicated for molecular clusters because of two reasons. First, the possibility of pronounced nuclear dynamics following the ionization process. Second, the possibility of complex intermolecular bonding patterns.

In this section, we investigate whether or not the molecular vibrations would make the spectra of molecular clusters more complicated. Methane is a good candidate for this study for two reasons. First, the monomer spectrum is highly structured. Second, intermolecular interactions in methane clusters are similar to those in rare-gas clusters. [1]

The carbon 1s photoelectron spectra for a beam of methane clusters and free monomers

[1] A methane molecules has a non-zero octupole. However, electrostatic interactions at the octupole level are unlikely to make a substantial contribution to the interaction energy.

are shown in Fig. 6.2. The monomer spectrum has been thoroughly investigated elsewhere (Karlsen and Børve 2000, Carroll et al. 1999). The cluster spectrum displays features that are characteristic of bulk and surface fractions. Moreover, it reveals a high-energy shoulder that has been attributed to the ν=1 vibrational excitation of the CH stretching mode in molecules in the surface layer. As far as we know, this is the first observation of resolved molecular vibrations in inner-shell photoelectron spectra of molecular clusters.

Interestingly, the surface-monomer and bulk-monomer shifts, obtained from experimental spectra, are close to what has been computed for argon clusters in the same size range. It thus seems that methane behaves similar to argon. This result is surprising but not unexpected, since the van der Waal parameters of methane are close to those of argon. [2]

The spectrum, in fig. 6.2, is fitted by two monomer lineshapes which are displaced in energy and further broadened by Gaussian distributions, which represent the contributions from bulk- and surface environments. From the fit, the surface spectrum is broader than the bulk spectrum. This may be due to a combined contribution from the distribution of ionization energies and intermolecular vibrations. From our experience with argon clusters, the contribution from intermolecular vibrations is expected to be negligible, and hence the width of the spectrum reflects the distribution of ionization energies. In light of these results, we explain the extra broadening of the surface spectrum as follows. In the surface layer, there are molecules with different coordination numbers. Upon ionization, these of course will have different charge screening, and accordingly different ionization energies.

This far, we have shown that molecular clusters with simple bonding mechanism display core-level photoelectron spectra which are in many ways similar to those of rare-gas clusters. Some features, though, may be less pronounced due to internal molecular vibrations, i.e. bulk-surface splitting. Now we go further and study core-level photoelectron spectra of molecular clusters with complex intermolecular bonding.

XPS lineshape models of methanol clusters

In this section, the attention is turned to hydrogen-bonded clusters, and in particular methanol clusters. We consider the carbon 1s photoelectron spectra of methanol clusters as well as the free monomers shown in fig. 6.3. The spectra of methane has been added for comparison.[3] At high ionization energy, the two spectra display very

[2]The effective Lennard-Jones potential well depths are 1.2 kJ/mol for argon dimer and 1.3 kJ/mol for methane dimer (Johnston 2002).

[3]The methane spectra presented in this section is different from the one analyzed in the previous section. The monomer contribution is now more pronounced.

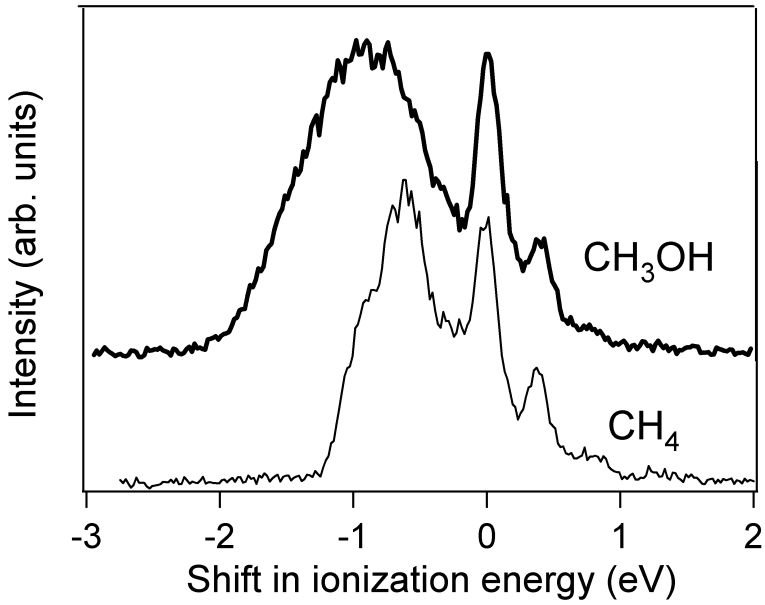

Figure 6.3: *Carbon 1s photoelectron spectra of methane and methanol clusters and monomers.*

similarly structured peaks corresponding to the free monomers. The parts of the spectra that correspond to the clusters are, by contrast, rather different. For methane, there are evidences for surface-bulk splitting and CH stretching, giving rise to both low and high-energy shoulders. By contrast, the spectrum of methanol clusters is broad and rather featureless. The difference between the spectra of methanol and methane clusters may be understood if we recognize that these clusters are characterized by different mechanisms of intermolecular bonding.

In order to analyze the spectrum of methanol clusters and interpret it in terms of chemical shifts and geometric structure of clusters, it is necessary to use theoretical lineshape models that represent well-defined bonding regimes in the cluster. We have longstanding experience with the development of this kind of models for rare-gas clusters. Our strategy has been to extend the methodology from rare-gas to molecular clusters. This has led to a breakthrough in this field, in that we have developed a general protocol for analyzing core spectra of molecular clusters, by combining classical simulations of clusters with single-molecule models from quantum mechanical calculations. The protocol employs molecular dynamics (MD) to simulate cluster geometries and a polarizable force field to calculate chemical shifts and line broadening due to excitation of intermolecular modes. The accuracy of the force-field approach has been verified based on comparisons with spectra of small clusters computed from first-principle theories.

This approach has been used to analyze the experimental spectra of methanol clusters. The spectrum, in fig. 6.4, has been disentangled into two model spectra that repre-

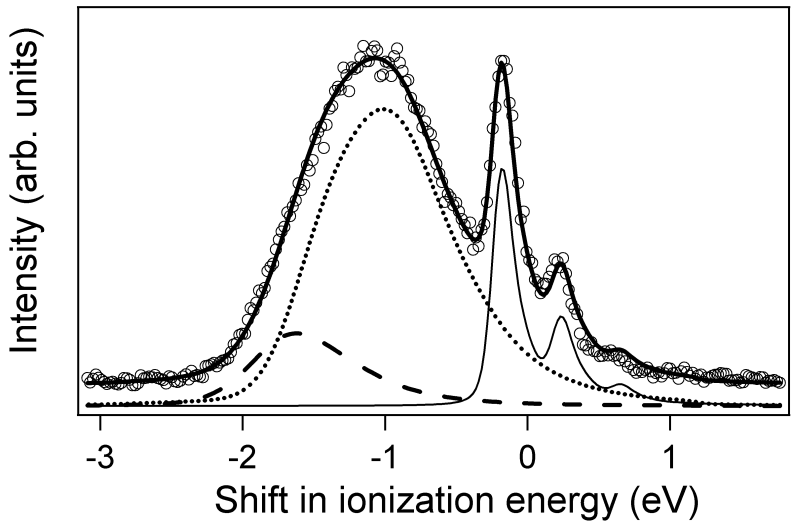

Figure 6.4: *C1s photoelectron spectrum of methanol clusters and the free molecule. Circles correspond to the experimental spectrum. The bold line corresponds to the theoretical spectrum. The dashed line corresponds to the bulk spectrum, the dotted line corresponds to the surface spectrum, and the thin line corresponds to spectrum of the free molecule.*

Table 6.1: *Peak parameters for bulk and surface spectra: chemical shifts relative to the free monomer (ΔIE) and its initial-state (ΔV) and final-state (ΔR) contributions, line broadening due to distribution of ionization energies (σ_1), and vibrational broadening due to excitation of intermolecular modes (σ_2), as obtained from theoretical calculations. All values are given in units of eV.*

	ΔIE	ΔV	ΔR	σ_1	σ_2
Bulk	-1.45	-0.21	1.23	0.50	0.28
Surface	-1.00	-0.22	0.78	1.00	0.25

sent two different bonding regimes in the cluster: bulk and surface. The model spectra used in this study correspond to the bulk and surface fractions of a cluster containing 200 methanol molecules simulated at T = 50 K. By inspecting the MD structures, the bulk spectrum corresponds to methanol molecules in linear and branched chains, whereas the surface spectrum corresponds to methanol molecules in rings and branched rings. The bulk- and surface-peak positions and linewidths are shown in Tab 6.1, as obtained from theoretical simulations. Our calculations reveal that these values will not change rapidly with size. This implies that the model spectra developed for one size may be useful as models for clusters in the same size range.

Regarding peak positions, cf Tab. 6.1, the bulk-monomer and surface-monomer chem-

ical shifts are -1.45 eV and -1.00 eV, respectively. The chemical shift may be divided into an initial-state contribution and a term due to final-state charge relaxation. The initial state effect arises due to specific nearest-neighbor interactions in terms of bonding, which give rise to substructures in the cluster, i.e. chains and rings. According to Tab. 6.1, the initial-state contribution to the chemical shift is small, and hence, the shift in ionization energy is mainly due to charge relaxation in the ionized state. The difference between the shifts for the bulk and the surface has been attributed to the reduced coordination at the surface, and the difference in cluster geometries between the bulk and the surface, i.e. chains vs rings.

Turning to peak linewidths, the surface spectrum has a linewidth twice that of the bulk spectrum. This difference arises due to different distribution of ionization energies and/or different values of vibrational broadening. According to Tab. 6.1, the contribution of vibrational broadening is minor, and hence the linewidth is mainly determined by the distribution of ionization energies. It follows that the extra broadening of the surface spectrum reflects the variations in coordination number in the surface layer.

Chapter 7

Conclusions

The main aim of this thesis is to develop novel computational models for analyzing inner-shell photoelectron spectra of free molecules and clusters, and to use these models to examine selected representative systems. Here, I would like to put in a few words what has been accomplished after three years of work.

The presence of a conformational equilibrium has been shown to affect an x-ray photoelectron spectrum significantly. In the particular case of ethanol, the conformational effect is expressed in the vibrational profiles; i.e. through the vibrational excitations accompanying the ionization process. Theoretical modeling is essential to make a definite identification and a quantitative interpretation of this effect. In this case, lineshape modeling is rather challenging because of the conformational change observed upon core ionization of the *gauche* ethanol. This results in large geometric relaxation to the extent that a coupled-mode treatment is required to get accurate lineshape models.

Lineshape modeling helps us improve our understanding of core-level photoelectron spectra of rare-gas and molecular clusters. We studied the Ar2p spectrum of argon clusters and carbon 1s spectra of methane and methanol clusters. The spectra of argon and methane clusters exhibit surface and bulk related features. On the contrary, the spectra of methanol clusters are broad and featureless. Theoretical lineshape models have been developed and used to interpret these spectra in terms of chemical shifts, intermolecular vibrations, and the local surrounding of atoms (molecules) in the cluster. It is found that the bulk-surface chemical shift can be explained as a result of different charge relaxation in the final state. The theoretical models predict the surface contribution at higher ionization energy, compared to the bulk contribution, because of the reduced coordination in the surface layer, and probably due to differences in the cluster geometries between the bulk and the surface (unique to methanol clusters). Second, the overall linewidth of the cluster spectrum is dominated by the distribution of ionization energies, which indicates that intermolecular vibrations are unlikely to make a substantial contribution to the cluster lineshape. Moreover, the surface peak is broader than the bulk peak because of the variations in the coordination number in the surface layer, compared to the bulk where all atoms (molecules) have equal coordination numbers.

Lineshape modeling emerges as an alternative approach for estimating the sizes of rare-gas clusters. By fitting lineshape models that are quantitatively accurate to the

experimental spectra of argon clusters, we have been able to provide estimate values of the mean cluster size.

In sum, we conclude that lineshape modeling has proven essential for our understanding of core-level photoelectron spectra of molecules with conformational equilibria, and clusters of rare-gas atoms and molecules. We hope that our results will contribute to the development of the current understanding of the structures and properties of molecules and clusters.

Bibliography

Allinger, N. L., Yuh, Y. H. and Lii, J.-H.: 1989, *J. Am. Chem. Soc.* **111**, 8551.

Amar, F. G., Smaby, J. and Preston, T. J.: 2005, *J. Chem. Phys.* **122**, 244717.

Ansbacher, F.: 1959, *Z. Naturforschg.* **14a**, 889.

Asplund, L., Gelius, U., Hedman, S., Helenelund, K., Siegbahn, K. and Siegbahn, P. E. M.: 1985, *J. Phys. B: At. Mol. Phys.* **18**, 1569.

Attfield, J. P., Johnston, R. L., Kroto, H. W. and Prassides, K.: 1999, New science from new material, *in* N. Hall (ed.), *The Age of Atoms and Molecules*, Royal Society of Chemistry, London, pp. 181–208.

Attwood, D. T.: 2000, *Soft X-rays and Extreme Ultraviolet Radiation*, Cambridge University Press.

Becke, A. D.: 1993, *J. Chem. Phys.* **98**, 5648.

Beeman, D.: 1976, *J. Comput. Phys.* **20**, 130.

Björneholm, O., Federmann, F., Fössing, F. and Möller, T.: 1995, *Phys. Rev. Lett.* **74**, 3017.

Björneholm, O., Federmann, F., Fössing, F., Möller, T. and Stampfli, P.: 1996, *J. Chem. Phys.* **104**, 1846.

Brooks, B. R.: 1988, *Algorithms for Molecular Dynamics at Constant Temperature and Pressure*, Internal Report of Division of Computer Research and Technology, National Institutes of Health.

Buck, U. and Krohne, R.: 1996, *J. Chem. Phys.* **105**, 5408.

Carroll, T. X., Berrah, N., Bozek, J., Hahne, J., Kukk, E., Sæthre, L. J. and Thomas, T. D.: 1999, *Phys. Rev. A* **59**, 3386.

Carroll, T. X., Thomas, T. D., Bergersen, H., Børve, K. J. and Sæthre, L. J.: 2006, *J. Org. Chem.* **71**, 1961.

Cederbaum, L. S. and Domcke, W.: 1976, *J. Chem. Phys.* **64**, 603.

Cramer, C. J.: 2002, *Essentials of Computational Chemistry*, John Wiley, New York.

Farges, J., de Feraudy, M. F., Raoult, B., and Torchet, G.: 1983, *J. Chem. Phys.* **78**, 5067.

Farges, J., de Feraudy, M. F., Raoult, B. and Torchet, G.: 1986, *J. Chem. Phys.* **84**, 3491.

Gelius, U., Svensson, S., Siegbahn, H., Basilier, E., Faxälv, Å. and Siegbahn, K.: 1974, *Chem. Phys. Lett.* **28**, 1.

Hagena, O. F.: 1987, *Z. Phys. D* **4**, 291.

Halgren, T. A.: 1992, *J. Am. Chem. Soc.* **114**, 7827.

Hartmann, E.: 1988, *J. Phys. B: At. Mol. Opt. Phys.* **21**, 1173.

Hergenhahn, U.: 2004, *J. Phys. B: At. Mol. Opt. Phys.* **37**, 89.

Hüfner, S.: 1996, *Photoelectron Spectroscopy*, Springer-Verlag, New York.

Johnston, R. L.: 2002, *Atomic and Molecular Clusters*, Masters series in physics and astronomy, Taylor and Francis, New York.

Jurvansuu, M.: 2000, *On The Experiments At The Gas Phase Beamline I411, MAX-LAB, SWEDEN*, University of Oulu, Finland.

Kakar, S., Björneholm, O., Weigelt, J., de Castro, A. R. B., Tröger, L., Frahm, R. and Möller, T.: 1997, *Phys. Rev. Lett.* **78**, 1675.

Kaker, R. K. and Quade, C. R.: 1980, *J. Chem. Phys.* **76**, 4300.

Karlsen, T. and Børve, K. J.: 2000, *J. Chem. Phys.* **112**, 7979.

Karnbach, R., Joppien, M., Stapelfeldt, J., Wörmer, J. and Möller, T.: 1993, *Rev. Sci. Instrum.* **64**, 2838.

Kempgens, B., Köppel, H., Kivimäki, A., Neeb, M., Cederbaum, L. S., and Bradshaw, A. M.: 1997, *Phys. Rev. Lett.* **79**, 3617.

Kiss, L. B., Söderlund, J., Niklasson, G. A. and Granqvist, C. G.: 1999, *Nanotechnology* **10**, 25.

Leach, A. R.: 2001, *Molecular Modeling, Principles and Applications*, Pearson Education Limited, Harlow.

Lee, C., Yang, W. and Parr, R. G.: 1988, *Phys. Rev. B* **37**, 785.

Lee, J. W. and Stein, G. D.: 1987, *J. Phys. Chem.* **91**, 2450.

Lindblad, A., Fink, R. F., Bergersen, H., Lundwall, M., Rander, T., Feifel, R., Öhrwall, G., Tchaplyguine, M., Hergenhahn, U., Svensson, S. and Björneholm, O.: 2005, *J. Chem. Phys.* **123**, 211101.

Luis, J. M., Bishop, D. M. and Kirtman, B.: 2004, *J. Chem. Phys.* **120**, 813.

Makri, N. and Miller, W. H.: 1987, *J. Chem. Phys.* **86**, 1451.

Mårtensson, N., Baltzer, P., Brühwiler, P. A., Forsell, J. O., Nilsson, A., Stenborg, A. and Wanneberg, B.: 1994, *J. Electron Spectrosc. Relat. Phenom.* **70**, 117.

Miller, W. H., Handy, N. C. and Adams, J. E.: 1980, *J. Chem. Phys.* **72**, 99.

Nyholm, R., Svensson, S., Nordgren, J. and Flodström, A.: 1986, *Nucl. Instrum. Methods Phys. Res. A* **246**, 267.

Parr, R. G. and Yang, W.: 1989, *Density Functional Theory of Atoms and Molecules*, Oxford University Press.

Petersen, H. and Baumgärtel, H.: 1980, *Nucl. Instrum. Methods* **172**, 191.

Ren, P. and Ponder, J. W.: 2002, *J. Comput. Chem.* **23**, 1497.

Ren, P. and Ponder, J. W.: 2003, *J. Phys. Chem. B* **107**, 5933.

Rennie, E. E., Hergenhahn, U., Kugeler, O., Rüdel, A., Marburger, S. and Bradshaw, A. M.: 2002, *J. Chem. Phys.* **117**, 6524.

Sæthre, L. J., Siggel, M. R. F. and Thomas, T. D.: 1989, *J. Electron Spectrosc. Relat. Phenom.* **49**, 119.

Schmid, G.: 1999, Nanosized clusters on and in support - perspectives for future catalysis, *in* P. Braunstein, L. A. Ora and P. R. Raithby (eds), *Metal Clusters in Chemistry*, Vol. 3, Wiley-VCH, Weinheim, pp. 1325–1341.

Senent, M. L., Smeyers, Y. G., Domínguez-Gómez, R. and Villa, M.: 2000, *J. Chem. Phys.* **112**, 5809.

Shaw, R. A., Wieser, H., Dutler, R. and Rauk, A.: 1989, *J. Am. Chem. Soc.* **112**, 5401.

Stampfli, P.: 1995, *Physics Reports* **255**, 1.

Stephens, P. J., Devlins, F. J., Chabalowski, C. F. and Frisch, M. J.: 1994, *J. Phys. Chem.* **98**, 11623.

Stevens, W. J., Basch, H. and Krauss, M.: 1984, *J. Chem. Phys.* **81**, 6026.

Stone, A. J.: 1981, *Chem. Phys. Lett.* **83**, 233.

Stone, A. J.: 2005, *J. Chem. Theory Comput.* **1**, 1128.

Svensson, S.: 2005, *J. Phys. B: At. Mol. Opt. Phys.* **38**, 821.

Svensson, S., Ausmees, A., Osborne, S. J., Bray, G., Gel'mukhanov, F., Ågren, H., de Brito, A. N., Sairanen, O. P., Kivimäki, A., Nömmiste, E., Aksela, H. and Aksela, S.: 1994, *Phys. Rev. Lett.* **72**, 3021.

Szabo, A. and Ostlund, N. S.: 1989, *Modern Quantum Chemistry*, McGraw-Hill.

Tanuma, S., Powell, C. J. and Penn, D. R.: 1994, *Surf. Interface Anal.* **21**, 165.

Tchaplyguine, M., Feifel, R., Marinho, R. R. T., Gisselbrecht, M., Sorensen, S. L., de Brito, A. N., Mårtensson, N., Svensson, S., and Björneholm, O.: 2003, *Chem. Phys.* **289**, 3.

Tchaplyguine, M., Marinho, R. R. T., Gisselbrecht, M., Schulz, J., Mårtensson, N., Sorensen, S. L., de Brito, A. N., Feifel, R., Öhrwall, G., Lundwall, M., Björneholm, O. and Svensson, S.: 2004, *J. Chem. Phys.* **120**, 345.

Thomas, T. D., Sæthre, L. J., Sorensen, S. L. and Svensson, S.: 1998, *J. Chem. Phys.* **109**, 1041.

Tromp, J. W. and Miller, W. H.: 1986, *J. Phys. Chem.* **90**, 3482.

van der Straten, P., Morgenstern, R. and Niehaus, A.: 1988, *Z. Phys. D* **8**, 35.

von Pietrowski, R., von Haeften, K., Laarmann, T., Möller, T., Museur, L. and Kanaev, A.: 2006, *Eur. Phys. J. D* **38**, 323.

Wilson, E. B., Decius, J. C. and Cross, P. C.: 1980, *Molecular vibrations*, Dover, chapter 2.5.

Xue, G.: 1993, *J. Global Optim.* **4**, 425.